The consequences of uncertainties in land use, climate and vegetation responses on the terrestrial carbon

Rik Leemans, Bas Eickhout, Bart Strengers, Lex Bouwman & Michiel Schaeffer

Institute of Public Health and the Environment, P.O. Box 1, 3720 BA Bilthoven, The Netherlands
Correspondence should be addressed to R. Leemans (email: rik.leemans@rivm.nl)

Received May 14, 2002

Abstract The IPCC SRES narratives were implemented in IMAGE 2.2 to evaluate the future condition of the climate system (including the biosphere). A series of scenario experiments was used to assess possible ranges in emissions and concentrations of greenhouse gases, climate change and impacts. These experiments focussed on the role of the terrestrial carbon cycle. The experiments show that the SRES narratives dominate human emissions and not natural processes. In contrary, atmospheric CO_2 concentration strongly differs between the experiments. Atmospheric CO_2 concentrations range for A1B from 714 to 1009 ppmv CO_2 in 2100. The spread of this range is comparable with the full SRES range as implemented in IMAGE 2.2 (515—895 μmol/mol CO_2). The most important negative and positive feedback processes in IMAGE 2.2 on the build-up of CO_2 concentrations are CO_2 fertilisation and soil respiration respectively. Indirect effects of these processes further change land-use patterns, deforestation rates and alter the natural C fluxes. The cumulative effects of these changes have a pronounced influence on the final CO_2 concentrations. Our scenario experiments highlight the importance of a proper parameterisation of feedback processes, C-cycle and land use in determining the future states of the climate system.

Keywords: carbon cycle, feedback processes, integrated assessment modeling, land use, SRES scenarios.

The Intergovernmental Panel on Climate Change (IPCC) has assessed the consequences of climate change[1, 2] using six Standardised Reference Emission Scenarios (SRES) [3]. These scenarios were based on qualitative, comprehensive narratives defined by two dimensions. The first dimension differentiates between 'material consumption' (A) and 'sustainability and equity' (B); the second between 'globalisation' (1) and 'regionalisation' (2). These dimensions specify typical characteristics and trends for each of the four quadrants (A1, B1, A2 and B2). Different combinations of energy carriers and energy efficiency further elaborated upon the A1 scenario. A1F uses only fossil fuels, A1B a balanced mix of fossil and renewables, and A1T is based on fuel-efficient technologies and renewables. The SRES CO_2 emissions range from 5 to 30 Pg C in 2100. These emissions lead to atmospheric CO_2 concentrations ranging from 540 to 970 μmol/mol[1]. When other GHGs and aerosols are added, the range in global temperature increase is 2.0 to 4.5 ^{o}C.

This range is a result of straightforward use of emissions scenarios in simple models of atmosphere, carbon (C) cycle and climate. Some uncertainties were considered. The uncertainty related to the climate sensitivity (i.e. the global mean warming at a doubled GHG-forcing) was

specifically assessed by IPCC and this widened the range of temperature increase to 1.4 to 5.8℃. Several papers have addressed the temperature, moisture and CO_2 sensitivity of major processes in the global C cycle[4, 5], and the influence of land-use change[6, 7] addressed some of the uncertainties of SRES but they did not consider land use and GHG emissions.

Major ecological processes determining the terrestrial C cycle are photosynthesis and respiration. Climate, CO_2 concentrations, soil conditions and species composition drive these processes. Furthermore, land-use change modifies these drivers. Feedback processes can have negative (slowing down the increase of atmospheric CO_2) or positive effects (accelerating the increase of atmospheric CO_2). The effects of feedback mechanisms on CO_2 concentrations can be substantial, particularly if their long-term effects are evaluated. For example, a small difference of 0.2 Pg C per year in C fluxes could lead cumulatively to 10-ppmv difference in concentrations over a century. The specific role of feedback processes remains uncertain.

In this paper we analyse these uncertainties further using the 'Integrated Model to Assess the Global Environment' (IMAGE 2.2) and our implementation of the SRES narratives[8, 9]. Different interactions and processes in IMAGE 2.2 can easily be varied. In this way, their relative importance can be determined. In this analysis, we focus on the influence of climate sensitivity, climate-change patterns and land-cover change on atmospheric CO_2 concentrations. In addition, we explore the impacts of feedback processes, which influence the terrestrial C cycle. This analysis is not a systematic sensitivity analysis, nor a comprehensive uncertainty analysis, because the richness of the SRES narratives, the complexity of the model and the available computing resources did not allow such analyses. Instead, we employed scenario experiments to estimate possible uncertainty ranges based on extreme assumptions.

First we give a brief description of IMAGE 2.2. The vegetation and C-cycle models are discussed in detail, since they are central to the analysis. Then we present the design of the experiments and discuss the results. We will show the necessity of an adequate parameterisation of the different feedback processes defining the dynamics of the terrestrial C cycle.

1 Model description

1.1 The structure of IMAGE 2.2

The objective of IMAGE-2.2 is to explore the long-term dynamics of global environmental change. IMAGE 2.2 has been extensively documented[10]. The main new elements of IMAGE 2.2 that differ from IMAGE 2.1 can be found in ref. [8]. The model consists of several modules (fig. 1). Interactions and several feedbacks are modelled explicitly.

General economic and demographic trends for 17 regions drive human activities. Regional energy consumption, energy efficiency improvements, fuel substitution, supply and trade of fossil fuels and renewable energy technologies determine energy production, energy use, industrial production, GHG emissions, ozone precursors and sulphur. Ecosystem, crop and land-use models are used to compute land use on the basis of regional consumption, production and trading of food,

animal feed, fodder, grass and timber, and local climatic and terrain properties. GHG emissions from land-use change, natural ecosystems and agricultural production systems and the exchange of CO_2 between terrestrial ecosystems and the atmosphere are determined. The atmospheric and ocean models calculate changes in atmospheric composition by employing the emissions and by taking oceanic CO_2 uptake and atmospheric chemistry into consideration. Subsequently, changes in climatic properties are computed by resolving oceanic heat transport and the changes in radiative forcing by GHGs and aerosols. The impact models involve specific models for sea-level rise and land degradation risk and make use of specific features of the ecosystem and crop models to depict impacts on vegetation.

Although IMAGE 2.2 is global in application, it performs many of its calculations on a terrestrial 0.5^0 by 0.5^0 grid (crop yields and crop distribution, land cover, land-use emissions and C cycle). IMAGE 2.2 integrates the regional socio-economic and gridded environmental dimensions.

Historical data for energy and industry CO_2 emissions[11] and concentrations[12] over the 1765—1970 period are used to spin up the C cycle and climate system. Data from many different sources are used to calibrate the energy, climate and land-use variables over a period from 1970 to 1995. IMAGE 2.2 scenario simulations cover the 1995—2100 period.

1.2 The vegetation and carbon models

The vegetation model and the terrestrial C model have been developed to simulate the consequences of changes in atmospheric CO_2 concentrations and climate on natural vegetation patterns, land cover and the terrestrial C cycle on the terrestrial grid. C uptake by the oceans is modelled in the oceanic C model (fig. 1). The vegetation model and the terrestrial C model require extensive data for initialisation and calibration. Each cell is characterised by its climate, land cover and soil. Climate-change anomalies are overlaid with the observed climatology by normalising a GCM-derived pattern with global mean temperature increase[13]. Throughout the simulations soil properties are assumed to be constant.

The vegetation model computes the potential distribution of natural vegetation and crops. The BIOME model[14] is used to determine the potential distribution biomes. A similar approach is used for crops and crop yield[15]. Biome patterns are updated every five years. Vegetation patterns change as a result of climate change, the atmospheric CO_2 concentration and migration of species. BIOME calculates an instantaneous equilibrium response to climate change by shifting biome patterns. In reality such shift takes time. Grasses migrate more rapidly than long-lived trees. The migration process is a function of the rate of climate change, original and new vegetation types and the distance to the nearest location where the new vegetation type already exists[16]. Vegetation patterns are also influenced by atmospheric CO_2 concentrations. Rising CO_2 concentrations increase water use efficiency (WUE). This allows plants to grow under more arid conditions. Enhanced WUE thus broadens the extent of forests and grasslands and decreases the extent of

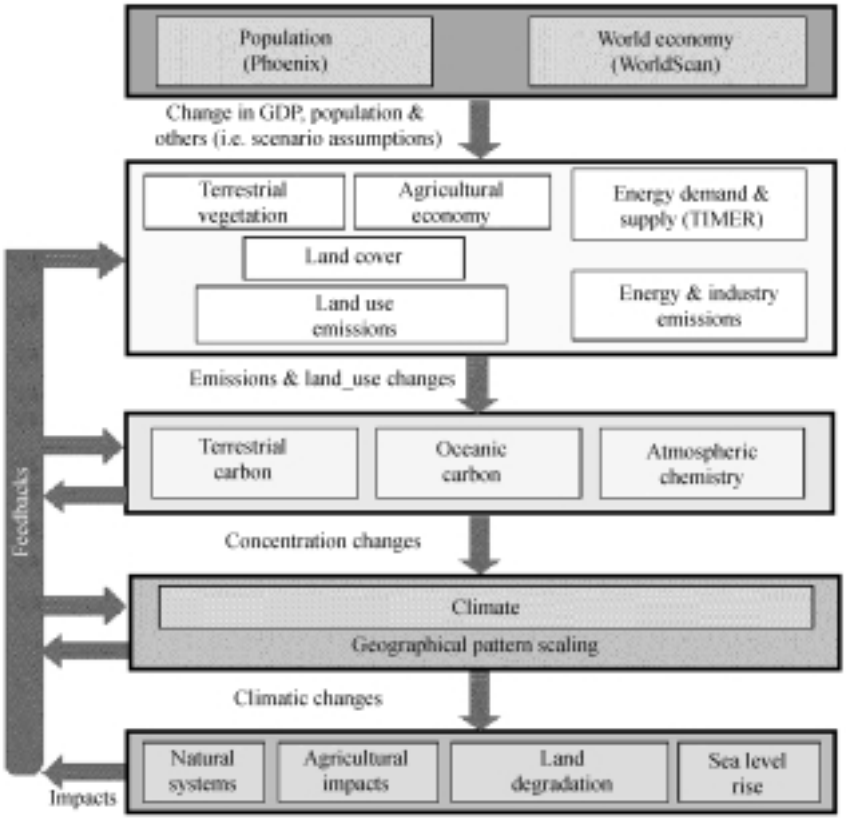

Fig. 1. The structure of IMAGE 2.2.

deserts.

The terrestrial C model simulates C fluxes between land and atmosphere, considering changes in atmospheric CO_2 concentrations, climate and the effects of land-cover change. The structure of the terrestrial C model is described by ref. [10]. A refined calibration has led to an improved parameter setting for the different land-cover types (table 1).

Net primary productivity (NPP) is calculated for every month and aggregated to an annual value. The actual value of NPP in any grid cell is a function of the land cover type, atmospheric CO_2 concentration, soil and climate:

$$NPP_j(t) = NPPI_{l_j} \cdot \sum_{m=1}^{12}\left(\left[1 + CF_{j,m}(t)\cdot \ln\left(\frac{[CO_2](t)}{[CO_2](1970)}\right)\right]\cdot \frac{f_1(T_{j,m}(t), l_j)\cdot f_2(SM_{j,m}(t))}{AF_{l_j}}\right), \quad (1)$$

$$CF_{j,m}(t) = 0.7 \cdot MIN\left(f_3(T_{j,m}(t), SM_{j,m}(t))\cdot f_4(l_j, N_j, A_j),\ 1.0\right), \quad (2)$$

Table 1

	NPP	Allocation fraction (–)				Life-time/a							Humification fraction
Land cover	/g •m^{-2} •a^{-1}	Leaves	Branches	Stems	Roots	Leaves	Branches	stems	roots	litter	humus	Charcoal	
Agricultural land	400	0.7	0.1	0	0.2	1	10	50	1	1	*	*	0.3
Extensive grasslands		0.6	0	0	0.4	1	10	50	1	1	*	*	0.3
Regrowth forests	Type dependent	*	*	*	*	*	*	*	*	*	*	*	*
Ice	0	0	0	0	0	0	0	0	0	0	0	0	0
Tundra	100	0.5	0.1	0.1	0.3	1	10	50	3	2	50	500	0.5
Wooded tundra	300	0.3	0.2	0.3	0.2	2	10	50	10	3	50	500	0.5
Boreal forest	500	0.3	0.2	0.3	0.2	2	10	50	10	3	50	500	0.6
Cool conifer forest	550	0.3	0.2	0.3	0.2	3	10	50	10	3	40	500	0.5
Temp. mixed forest	600	0.3	0.2	0.3	0.2	2	10	50	10	2	40	500	0.5
Temperate deciduous forest	650	0.3	0.2	0.3	0.2	1	10	50	10	2	40	500	0.4
Warm mixed forest	650	0.3	0.2	0.3	0.2	1	10	50	10	2	40	500	0.4
Steppe	450	0.6	0	0	0.4	1	10	50	2	1	30	500	0.4
Hot desert	50	0.6	0	0	0.4	1	10	50	2	1	50	500	0.4
Scrubland	400	0.3	0.2	0.2	0.3	1	10	30	5	2	30	500	0.4
Savanna	500	0.3	0.2	0.2	0.3	1	10	30	5	2	20	500	0.4
Tropical woodland	900	0.3	0.2	0.3	0.2	1	10	30	10	2	20	500	0.4
Tropical forests	1200	0.3	0.2	0.3	0.2	1	10	30	10	2	20	500	0.4

* Values of underlying natural vegetation type are used.

$$AF_{l_j} = \frac{\sum_{i \wedge i \in l} \left(\sum_{m=1}^{12} \left(f_1(T_{i,m}(1970), l_i) \cdot f_2(SM_{i,m}(1970)) \right) \right) \cdot area_i}{\sum_{i \wedge i \in l} area_i}, \quad (3)$$

where t = time (1970—2100); j = grid-cell index (1—66,663); m = month index (1—12); l = land-cover index (1—19); i = index of all grid cells in one land-cover type in 1970 (subset of j); NPP = net primary production (Mg C/km^2); $NPPI$ = mean NPP of one land-cover type in 1970 (Mg C/km^2); CF = CO_2 fertilisation factor (–); [CO_2]= CO_2 concentration (μmol/mol); T = monthly temperature (℃); SM = monthly soil-water status (%); f_1 = multiplier for direct temperature effect on plant growth (–); f_2 = multiplier for water availability effect on plant growth (–); f_3 = correction function for temperature and soil water status on CO_2 fertilisation (–); f_4 = correction factor for species characteristics (l), nutrient availability (N) and altitude (A) on CO_2 fertilisation (–); AF= normalisation factor to 1970 average (–); $area$ = grid-cell area (km^2).

NPP is divided into their living biomass (leaves, branches, stems, roots), non-living biomass (litter, humus and charcoal) and forest products (timber, fibre and pulp) components. Living biomass is transformed into litter on the basis of land-cover specific life times. Litter finds its way to humus (humification factor) and inert soil C (charcoal, 6% per year), using humification and carbonisation fractions. During the various transformations part of the C is lost to the atmosphere in the form of CO_2 through soil respiration of litter and humus, which is computed as a function of soil temperature and soil moisture.

The terrestrial C model explicitly deals with four land-cover transitions: (i) natural vegetation to agricultural land (either cropland or pasture), (ii) agricultural land to other land-cover types because of the abandonment of agricultural land, (iii) forests to 'regrowth forests' because of timber extraction, and (iv) conversion of one type of natural vegetation to another because of environmental change.

2 Simulation experiments

The first set of scenarios is the six SRES narratives[3] implemented in IMAGE 2.2. These scenarios are labelled A1F, A1B, A1T, A2, B1 and B2. All these scenarios are based on a medium climate sensitivity (2.5℃) and use the climate-change patterns derived from the GCM of the Hadley Centre (HADCM2)[17].

We selected the A1B scenario as the reference scenario for this analysis because it shows a mix of different fuels, average land use activities and deforestation and, consequently, intermediate emissions. To determine the sensitivity of using different climate change patterns the results from other GCM-simulations than HADCM2 were used. Incorporation of the different climate change patterns (temperature and precipitation change) lead to different crop productivities,

land-use patterns, ecosystem shifts and regional C fluxes. Many of those are triggered by changes in moisture availability. The GCMs used are ECHAM-4[18] (A1B_ECHAM4), CGCM-1[19] (A1B_CGCM1), CSIRO-MK12[20] (A1B_CSIROMK2) and GFDL-LR[21] (A1B_GFDLLR). Detailed information on the GCM-simulations can be found on the web site of the IPCC Data Distribution Centre (ipcc-ddc.cru.eea.ac.uk). The differences in impacts are greater regionally than globally.

IPCC calculated the global mean temperature increase since 1990 with different climate sensitivities. Here we repeat this exercise for different SRES narratives. A1F is the scenario with the highest emissions, while B1 shows the lowest emissions (see table 2). A1F with high climate sensitivity (A1F_high) and B1 with low climate sensitivity (B1_low) together span the range of global mean temperature. 'A1B_low' and ‘A1B_high' are presented for completeness because it is the reference scenario used throughout this paper.

Table 2 Total emissions stemming from human activities for the different scenario experiments

	CO_2 emissions in 2050 (in Pg C/a)	CO_2 emissions in 2100 (in Pg C/a)	CO_2-equivalent emissions in 2050 (in Pg C/a)	CO_2-equivalent emissions in 2100 (in Pg C/a)
A1F	25.3	29.1	31.1	34.2
A1B	22.6	17.7	28.3	22.2
A1T	19.1	11.9	24.6	16.2
A2	18.5	31.0	24.0	39.3
B1	13.4	6.2	17.4	8.9
B2	13.1	12.7	17.7	17.6
A1B_ECHAM4	22.4	17.7	28.1	22.3
A1B_CGCM1	22.6	17.7	28.3	22.2
A1B_CSIROMK2	22.4	17.6	28.1	22.2
A1B_ GFDLLR	22.5	17.7	28.2	22.3
A1B_low	22.5	17.6	28.2	22.5
A1B_high	22.7	17.6	28.4	22.2
A1F_low	25.3	29.1	31.0	34.1
A1F_high	25.4	29.1	31.1	35.2
B1_low	13.2	6.2	17.2	9.0
B1_high	13.3	6.2	17.3	8.9
A1B_constfert	22.7	17.4	28.5	22.0
A1B_constwue	22.6	17.6	28.4	22.2
A1B_constresp	22.6	17.6	28.3	22.2
A1B_consttempgrowth	22.7	17.6	28.4	22.1
A1B_nomigration	22.6	17.6	28.3	22.2
A1B_fastmigration	22.7	17.7	28.4	22.3
A1B_constclim	22.3	17.7	28.0	22.2
A1B_nonegfb	22.8	17.2	28.6	22.0
A1B_noposfb	22.5	17.7	28.2	22.3

IMAGE 2.2 distinguishes two direct effects of CO_2 on plant growth. The first is CO_2 fertilisation, which enhances photosynthesis. The resulting increase of NPP (eqs. (1) and (2)) results in a slower build-up of CO_2 in the atmosphere. CO_2 fertilisation is thus a negative feedback. In the scenario 'A1B_constfert' no additional CO_2 fertilisation is assumed after 1995. The second direct CO_2 effect is enhanced WUE. The result is that NPP and the net uptake of C increases, especially in drier conditions. Therefore, on average, it also is a negative feedback. To show its impact this effect is held constant in the 'A1B_constwue' scenario from 1995.

Climate change is an indirect effect of changing CO_2 and other GHG concentrations, which together constitute the so-called CO_2-equivalent concentrations (including CO_2, CH_4, N_2O, HFCs, PFCs and SF6; table 4). Here we focus strongly on two temperature-related feedbacks: soil respiration and plant growth. Soil respiration increases exponentially with increasing temperatures, provided that there is enough soil moisture, increasing the CO_2-flux to the atmosphere (a positive feedback). In the 'A1B_constresp' scenario, we kept the soil respiration rates constant at 1995 values. The temperature-response function on plant growth is more complex with an optimum, a minimum and maximum threshold. In the 'A1B_consttempgrowth' scenario we have kept the temperature effect on plant growth at its 1995 value. This feedback turns out to be negative globally.

Climate change also influences the distribution of plants. Here both changes in temperature and precipitation are important. The dynamics of these distributional shifts are often not immediate. We have made two extreme assumptions: instantaneous transition (A1B_fastmigration) and no transition (A1B_nomigration). The first is a negative feedback because rapidly pole-wards shifting forests result in more C being stored. The second is a positive feedback because less C is stored.

Table 3 Terrestrial carbon fluxes to the atmosphere (positive) for the different scenario experiments. The net flux results from C uptake in natural vegetation and deforestation fluxes.

	C uptake in 2050 (in Pg C/a)	C uptake in 2100 (in Pg C/a)	Net flux in 2050 (in Pg C/a)	Net flux in 2100 (in Pg C/a)
A1B	–5.9	–7.5	–3.6	–5.3
A1B_constfert	–1.2	–2.1	1.7	–0.2
A1B_constwue	–6.0	–7.0	–3.1	–4.9
A1B_constresp	–7.2	–8.8	–4.3	–6.7
A1B_consttempgrowth	–5.2	–6.3	–2.3	–4.1
A1B_nomigration	–5.5	–5.9	–2.7	–3.8
A1B_fastmigration	–6.7	–8.1	–3.7	–5.8
A1B_constclim	–6.0	–7.3	–3.4	–5.1
A1B_nonegfb	1.1	0.8	4.3	2.5
A1B_noposfb	–7.1	–8.7	–4.3	–6.5

Table 4 Atmospheric and climate characteristics in 2100 of the different scenario experiments

	Atmospheric CO_2 concentrations/μmol • mol^{-1}	Atmospheric CO_2–equivalent concentrations/ μmol • mol^{-1}	Global-mean temperature change since pre-industrial times/^oC
A1F	895	1231	3.7
A1B	755	1032	3.4
A1T	645	901	3.2
A2	871	1315	3.7
B1	515	639	2.3
B2	606	821	2.9
A1B_ECHAM4	754	1032	3.4
A1B_CGCM1	761	1037	3.5
A1B_CSIROMK2	747	1021	3.4
A1B_ GFDLLR	749	1024	3.4
A1B_low	747	1019	2.3
A1B_high	775	1062	5.1
A1F_low	884	1201	2.5
A1F_high	916	1251	5.4
B1_low	512	628	1.5
B1_high	523	643	3.5
A1B_constfert	918	1244	3.9
A1B_constwue	765	1046	3.5
A1B_constresp	723	987	3.3
A1B_consttempgrowth	792	1081	3.6
A1B_nomigration	784	1071	3.5
A1B_fastmigration	739	1010	3.4
A1B_constclim	760	1030	0.4
A1B_nonegfb	1009	1368	6.0
A1B_noposfb	714	973	2.2

Finally, we have added three combined runs with a constant climate after 1995 (A1B_constclim: no temperature and precipitation change), no negative feedbacks (A1B_nonegfb: no CO_2 fertilisation, no temperature effect on plant growth, high climate sensitivity, no enhanced WUE and no migration) and no positive feedbacks (A1B_noposfb: low climate sensitivity, no change in soil respiration and instantaneous migration). These combined runs allow assessing the full sensitivity range of the experiments.

3 Results and discussion

The globally aggregated results for the SRES narratives, the different climate change patterns, the different climate sensitivities and the feedback experiments are summarised in tables 2—5 and figs. 2—5 and Plate I. The CO_2 emissions and CO_2-equivalent emissions stemming from human activities in the SRES narratives vary between 6.2 and 31.0 and 8.9 and 39.3 Pg C respectively in 2100 (table 2). The non-CO_2 GHGs are more important in scenarios with lower CO_2 emissions (A1T, B1 and B2). Over the years, the scenarios follow different pathways (see fig. 2). Generally, emissions increase initially and decline thereafter. Only A1F and A2 show a continuous increase, which results in the highest emissions in 2100. The two B-scenarios (B1 and B2) have the lowest

Table 5 The extent (Mha) of different land uses for the different scenario experiments in 2100

	Food crops	Grass and fodder crops	Biofuel crops	Forests
A1F	1420	2310	700	5370
A1B	1490	2350	1040	4980
A1T	1500	2370	1010	4960
A2	2600	3640	670	3430
B1	1260	2140	370	5750
B2	1660	2820	710	4800
A1B_ECHAM4	1510	2350	1040	5030
A1B_CGCM1	1480	2390	1060	4950
A1B_CSIROMK2	1480	2320	1010	5070
A1B_ GFDLLR	1490	2330	1030	5040
A1B_low	1460	2360	1020	4970
A1B_high	1560	2380	1080	4920
A1F_low	1390	2310	690	5360
A1F_high	1490	2350	720	5300
B1-low	1240	2150	370	5710
B1-high	1290	2150	380	5770
A1B_constfert	1780	2520	1200	4540
A1B_constwue	1480	2350	1040	4750
A1B_constresp	1490	2360	1050	4960
A1B_consttempgrowth	1480	2350	1030	5010
A1B_nomigration	1480	2350	1030	4550
A1B_fastmigration	1490	2350	1040	5220
A1B_constclim	1390	2370	1020	4810
A1B_nonegfb	1900	2590	1280	3890
A1B_noposfb	1460	2360	1030	5120

emissions. Emissions of CO_2 and other GHGs do not change much with low or high climate sensitivity, different climate patterns or feedbacks (fig. 2). The difference in emission range between all experiments is less than 0.5 Pg C per year. CO_2 emissions are dominated by emissions related to the burning of fossil fuels. Separating the emission calculations from the simulation of other processes in the earth system still lead to robust estimates.

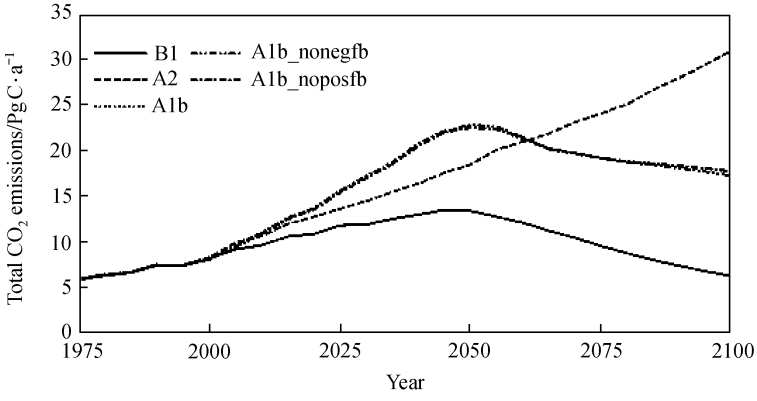

Fig. 2. Annual CO_2 emissions (in Pg C) for the A2 and B1 SRES narrative that define the range. The lowest and highest emission of the scenario experiments are A1B_constresp and A1B_nonegfb.

The terrestrial C fluxes, however, strongly differ between the different scenarios (table 3). Natural vegetation currently sequesters C. In the original A1B scenario this sequestration is enhanced over time. In the different experiments the terrestrial C flux strongly varies. In some of the scenarios (A1B_constfert and A1B_nonegfb) natural vegetation becomes a source. The simulated range of 8.2 Pg C and 9.5 Pg C in 2050 and 2100 respectively is large in comparison with the differences in deforestation fluxes (2.3—3.0 Pg C and 1.7—2.3 Pg C in 2050 and 2100 respectively). This clearly indicates the importance of the role of natural vegetation in the global C cycle.

Although emissions do not substantially differ, the subsequent natural C-fluxes cause large variation in atmospheric CO_2 concentrations (table 4). The potential differences in concentrations are almost as large as the original SRES range (fig. 3). This is caused by the cumulative effect of small changes in C uptake by vegetation (table 3). The most important feedback is CO_2 fertilisation (from 755 to 918). Constant CO_2 fertilisation rapidly stabilises NPP. Other experiments show much smaller impacts. The results further show that the impact of constant soil respiration is much less than that of CO_2 fertilisation. Although, soil respiration is the largest positive feedback, CO_2 fertilisation more strongly determines the final atmospheric CO_2 concentrations.

The combined effect of disabling all negative feedbacks (A1B_nonegfb) results in a CO_2 concentration of 1009 μmol/mol, which is 254 μmol/mol higher than in the reference scenario (A1B). Notice that this increase is comparable to the sum of all the individual effects in isolation.

Table 5 illustrates some of the land-use consequences of these scenario experiments. There are large differences in land use among the original SRES narratives, which is driven by the

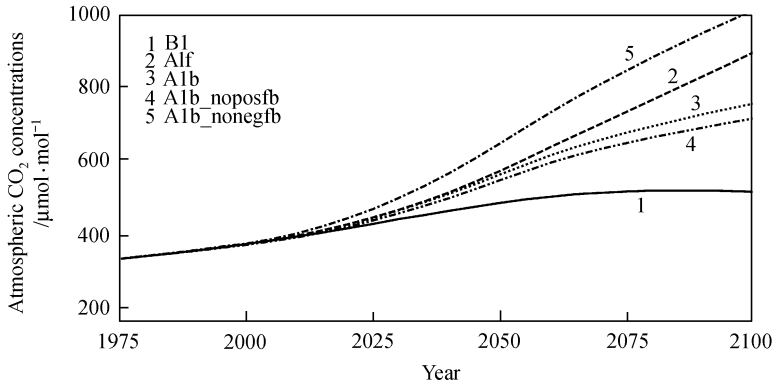

Fig. 3. Atmospheric CO_2 concentrations. B1 and A1f gives the range of all default SRES narratives, while the dashed lines provide the range of A1B scenario experiments.

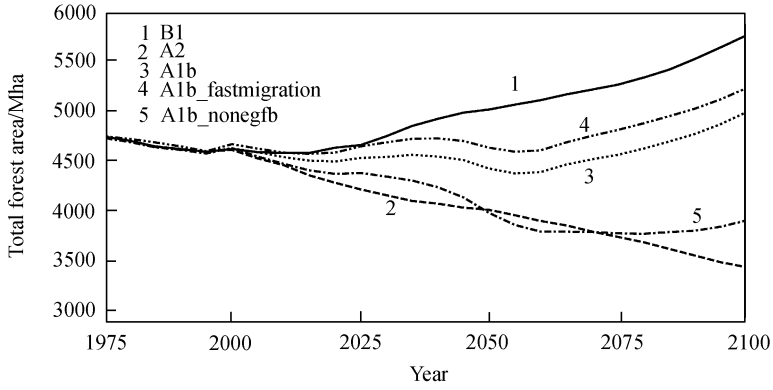

Fig. 4. Total forest area. A1 and B1 give the range of all default SRES narratives, while the rest of the lines provide the range of A1B scenario experiments.

different assumptions in the narratives (population, wealth, trade, diet, energy source, etc.). The regional differences between the land-use patterns in the scenarios [8] are large but a discussion is beyond the scope of this paper. In the scenarios with the different GCMs there is globally only a small difference in the change of forest extent. However, it determines the size of the terrestrial C pool, which influences atmospheric concentrations (see table 4).

The impact on forest extent is much more pronounced when the different feedback processes are considered (table 5 and fig. 4). The range is here 3890—5220 Mha in 2100 (c.f. 4590 Mha in 1995), which means that in some of the experiments the noticeable forestation worldwide in the A1B scenario is reversed. This leads to additional land-use emissions from deforestation. The lowest forest-extent value is obtained when all negative feedbacks are switched off (the 'A1B_nonegfb' scenario). The direct CO_2 and climate effects on crop growth explain this decline. Crops generally are well fertilised, grow in regions with adequate moisture supply, leading to a pronounced CO_2-fertilisation effect. Without CO_2-fertilisation, crop yields decline and more land is needed to grow crops. The experiments clearly show that the simulated forest extent can easily

shift from an increase to a decrease, which has large implications for environmental policies. The impacts of feedback processes on land use are pronounced and influence the C fluxes related to deforestation and forestation. The selection of A1B for the uncertainty experiments, however, clearly shows the sensitivity of forestation and deforestation.

The results from these experiments indicate that besides direct effects, there are also indirect effects. One of those indirect effects is the land-use consequences of increased productivity of agricultural crops due to CO_2-fertilisation. An additional 620 Mha (290 for food crops, 170 for grassland and 160 for biofuels) is needed to satisfy land-use demand in A1B_constfert, which results in a decrease of 440 Mha in forest extent (table 5 and fig. 4). Here this indirect effect of CO_2-fertilisation convincingly increases the impact of this negative feedback through land-use. The land-use consequences should thus be considered. Other indirect effects are probably less pronounced but can alter concentrations.

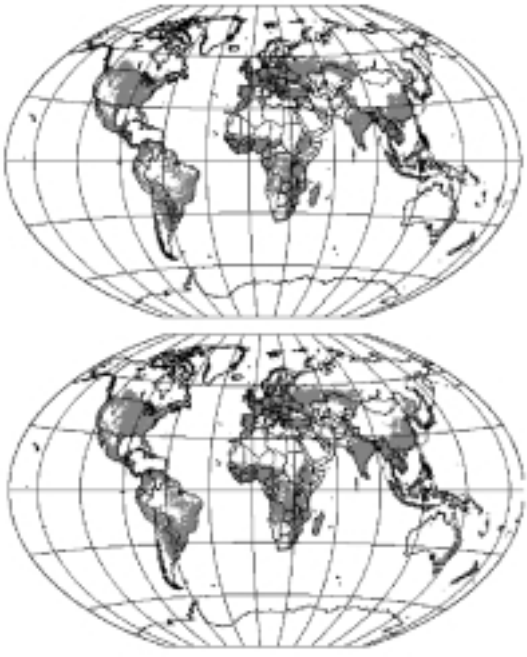

Fig. 5. Agricultural land in 2050 for the two extremes in the scenario experiments (A1B_constclim and A1B_nonegfb).

Changes in C fluxes influence the concentrations at the end of this century (table 4 and fig. 3). The range of CO_2 concentrations in 2100 for the different SRES narratives is 515—895 μmol/mol CO_2, with A1B at 755 μmol/mol CO_2. Including also other GHGs, which is important to determine the impact on radiative forcing and thus climate, increases the range to 640 — 1315 μmol/mol CO_2-equivalent. The range of the scenario experiments based on A1B is 715 to 1010 μmol/mol and 975 to 1370 μmol/mol for CO_2 and CO_2-equivalent concentrations respectively. The upper limit of the range clearly goes beyond the range of the original SRES narratives. These ranges are also reflected in the different changes in global mean temperatures (table 4).

The resulting climate change (table 4) shows the consequences for C fluxes between the experiments. The warming induces pole-ward shifts in potential distributions of crops and other plants, influencing land-use and vegetation patterns (fig. 5 and Plate I). This redistribution has also an impact on C fluxes. The impacts of climate change are presented in several scenario experiments (A1B_nomigration, A1B_fastmigration and A1B_constclim). The forest extent is largest in the A1_fastmigration scenario (table 5). Here, large parts of the Polar Regions rapidly shift from

tundra-like vegetation to boreal forests, sequestering additional C. This scenario shows one of the lowest atmospheric concentrations. Unfortunately, such immediate response is an unrealistic assumption.

The agricultural extent is lowest in the A1B_constclim scenario. In this experiment the positive effects of CO_2-fertilisation are combined with a reduction of negative climate-change effects (mainly changes in moisture). Such an agricultural extent lead to smaller deforestation fluxes than in the other experiment but not to a large increase in C uptake in natural vegetation. This is due to the absence of vegetation shifts due to climate change. These shifts are responsible for a large fraction of the additional C uptake in the scenario. This is another example of an indirect effect as discussed above.

4 Concluding remarks

We have used a series of scenario experiments to assess the possible ranges in emissions, concentrations and climate change. However, assuming no direct-CO_2 effects, no climate dependency of ecological processes, and unlimited and immediate vegetation redistribution are certainly unrealistic. Our results show that results can easily be manipulated by neglecting important processes and interactions. This paper is instrumental in highlighting the importance of comprehensive state-of-the-art integrated approaches.

The emission pathways are the most widely used aspect of SRES. Our analysis shows that the SRES narratives dominate human GHG emissions and that these are not strongly influenced by other processes. There are only minor differences in emissions in our scenario experiments. This finding is encouraging for the way that the IPCC has set up her assessment (developing emission scenarios separately from climate-change and impact assessments) and allows further refinement of local and regional emission scenarios, without accounting for global processes further down the causal chain.

Our analysis further clearly shows that this independence falls apart when the subsequent components of the climate system are considered. Atmospheric GHG concentrations, radiative forcing, climate change and vegetation responses strongly interact and cannot be considered in isolation. This finding is consistent with the conclusion of ref. [5] and ref. [7]. The added value of this study is that also the impact on human GHG emissions and the role of indirect effects are considered. These indirect effects change land-use patterns, deforestation rates and alter the C fluxes of natural vegetations. We have shown that the cumulative effects of these changes have a pronounced influence on the final concentrations.

The default simulations of IMAGE 2.2 assume adequate settings for model parameters, based on experimental evidence and literature reviews. The IMAGE 2.2 results for the SRES narratives therefore provide a probable outcome because many direct and indirect effects are considered.

Acknowledgements We appreciate the constructive reviews of Joos and Levi, which improved the manuscript considerably. The research was initiated as part of the CARBONSINK-LBA project funded by EU-DGXII (EVK2-CT1999-00023), to test if global emissions scenarios could be used for regional assessments.

References

1. Houghton, J. T., Ding, Y., Griggs, D. et al., editors, Climate Change 2001, The Science of Climate Change, Cambridge: Cambridge University Press, 2001.
2. McCarthy, J. J., Canziani, O. F., Leary, N. et al., editors, Climate Change, Impacts, Adaptation and Vulnerability, Cambridge: Cambridge University Press, 2001.
3. Nakícenovíc, N., Alcamo, J., Davis, G. et al., Special Report on Emissions Scenarios, Cambridge: Cambridge University Press, 2000.
4. Schimel, D. S., Emanuel, W., Rizzo, B. et al., Continental scale variability in ecosystem processes: models, data, and the role of disturbance, Ecological Monographs, 1997, 67: 251—271.
5. Cox, P. M., Betts, R. A., Jones, C. D. et al., Acceleration of global warming due to carbon-cycle feedbacks in a coupled climate model, Nature, 2000, 408: 180—184.
6. Houghton, R. A., Hackler, J. L., Lawrence, K. T., The US carbon budget: Contributions from land-use change, Science, 1999, 285: 574—578.
7. Joos, F., Prentice, I. C., Sitch, S. et al., Global warming feedbacks on terrestrial carbon uptake under the Intergovernmental Panel on Climate Change (IPCC) emission scenarios, Global Biogeochemical Cycles, 2001, 15: 891–907.
8. IMAGE team, The IMAGE 2.2 implementation of the SRES scenarios: A comprehensive analysis of emissions, climate change and impacts in the 21st century, RIVM CD-ROM Publication 481508018, Bilthoven: National Institute of Public Health and the Environment, 2001.
9. IMAGE team, The IMAGE 2.2 implementation of the SRES scenarios: Climate change scenarios resulting from runs with several GCMs, RIVM CD-ROM Publication 481508019, Bilthoven: National Institute of Public Health and the Environment, 2001.
10. Alcamo, J., Leemans, R., Kreileman, G. J. J., Global change scenarios of the 21st century, Results From the IMAGE 2.1 Model, London: Pergamon & Elseviers Science, 1998.
11. Marland, G., Boden, T. A., Global, regional, and national CO_2 emissions, in Trends: A Compendium of Data on Global Change, Oak Ridge: Carbon Dioxide Information Analysis Center, Oak Ridge National Laboratory, 2000.
12. Keeling, C. D., Whorf, T. P., Atmospheric CO_2 records from sites in the SIO air sampling network, in Trends: A Compendium of Data on Global Change, Oak Ridge, Tenn., U.S.A.: Carbon Dioxide Information Analysis Center, Oak Ridge National Laboratory, 2001.
13. Schlesinger, M. E., Malyshev, S., Rozanov, E. V. et al., Geographical distributions of temperature change for scenarios of greenhouse gas and sulfur dioxide emissions, Technological Forecasting and Social Change, 2000, 65: 167—193.
14. Prentice, I. C., Cramer, W. P., Harrison, S. P. et al., A global biome model based on plant physiology and dominance, soil properties and climate, Journal of Biogeography, 1992, 19:117—134.
15. Leemans, R., van den Born, G.-J., Determining the potential global distribution of natural vegetation, crops and agricultural productivity, Water, Air and Soil Pollution, 1994, 76: 133—161.
16. van Minnen, J. G., Leemans, R., Ihle, F., Defining the importance of including transient ecosystem responses to simulate C-cycle dynamics in a global change model, Global Change Biology, 2000, 6: 595—612.
17. Mitchell, J. F. B., Johns, T. C., Gregory, J. M. et al., Climate response to increasing levels of greenhouse gases and sul-

phate aerosols, Nature, 1995, 376: 501—504.

18. Bacher, A., Oberhuber, J. M., Roeckner, E., ENSO dynamics and seasonal cycle in the tropical Pacific as simulated by the ECHAM4/OPYC3 coupled general circulation model, Climate Dynamics, 1998, 14: 431—450.
19. Boer, G. J., Flato, G. M., Reader, M. C. et al., A transient climate change simulation with greenhouse gas and aerosol forcing: experimental design and comparison with the instrumental record for the twentieth century, Climate Dynamics, 2000, 16: 405—425.
20. Hirst, A. C., Gordon, H. B., O'Farrell, S. P., Global warming in a coupled climate model including oceanic eddy-induced advection, Geophysical Research Letters, 1996, 23: 3361—3364.
21. Haywood, J. M., Stouffer, R. J., Wetherald, R. T. et al., Transient response of a coupled model to estimated changes in greenhouse gas and sulfate concentrations, Geophysical Research Letters, 1997, 24: 1335—1338.

Natural vegetation patterns in 2100 for the two extremes in the scenario experiments: A1B_fastmigration (top) and A1B_nonegfb (bottom).